^{4}He and 99% of Ne will be released from IDPs within 10^5 years, even at 100°C and 200°C, respectively. Because an oceanic plate moves at a speed of 1 to 10 cm/year, or only 1 to 10 km in 10^5 years, the above calculation shows a possibility that solar He and Ne in IDPs would be released at the very beginning of subduction [at a depth of <12 km for 100°C and <24 km for 200°C (*31*)]. At such shallow depths in subduction zones, the solar-type He and Ne released from IDPs would be easily carried away with fluids and lost from the subducting slabs. If this is the case, the solar Ne and ^{3}He observed in the mantle-derived samples is unlikely to be the result of subduction of IDP grains but should be considered as reflecting a primordial noble gas component in the mantle.

REFERENCES AND NOTES

1. H. Craig and J. E. Lupton, *Earth Planet. Sci. Lett.* **31**, 369 (1976).
2. R. Poreda and F. R. Brozolo, *ibid.* **69**, 277 (1984); P. Sarda, T. Staudacher, C. J. Allègre, *ibid.* **91**, 73 (1988); B. Marty, *ibid.* **94**, 45 (1989).
3. H. Hiyagon, M. Ozima, B. Marty, S. Zashu, H. Sakai, *Geochim. Cosmochim. Acta* **56**, 1301 (1992).
4. M. Honda, I. McDougall, D. B. Patterson, A. Doulgeris, D. A. Clague, *Nature* **349**, 149 (1991); *Geochim. Cosmochim. Acta* **57**, 859 (1993).
5. T. K. Kyser and W. Rison, *J. Geophys. Res.* **87**, 5611 (1982); R. J. Poreda and K. A. Farley, *Earth Planet. Sci. Lett.* **113**, 129 (1992).
6. M. Honda, J. H. Reynolds, E. Roedder, S. Epstein, *J. Geophys. Res.* **92**, 12507 (1987); M. Ozima and S. Zashu, *Geochim. Cosmochim. Acta* **52**, 19 (1988); *Earth Planet. Sci. Lett.* **105**, 13 (1991).
7. D. Phinney, J. Tennyson, U. Frick, *J. Geophys. Res.* **83**, 2313 (1978); M. W. Caffee *et al.*, *Lunar Planet. Sci.* **XIX**, 154 (1988).
8. B. M. Kennedy, M. A. Lynch, J. H. Reynolds, S. P. Smith, *Geochim. Cosmochim. Acta* **49**, 1251 (1985).
9. R. S. Rajan *et al.*, *Nature* **267**, 133 (1977).
10. A. O. Nier and D. J. Schlutter, *Lunar Planet. Sci.* **20**, 790 (1989); C. T. Olinger, M. Maurette, R. M. Walker, C. M. Hohenberg, *Earth Planet. Sci. Lett.* **100**, 77 (1990).
11. A. Ya. Krylov, B. A. Mamyrin, Yu. I. Silin, L. V. Khabarin, *Geochem. Int.* **10**, 202 (1973).
12. M. Ozima, M. Takayanagi, S. Zashu, S. Amari, *Nature* **311**, 448 (1984).
13. S. Amari and M. Ozima, *ibid.* **317**, 520 (1985).
14. H. Fukumoto, K. Nagao, J. Matsuda, *Geochim. Cosmochim. Acta* **50**, 2245 (1986).
15. M. Takayanagi and M. Ozima, *J. Geophys. Res.* **92**, 12531 (1987).
16. S. Amari and M. Ozima, *Geochim. Cosmochim. Acta* **52**, 1087 (1988).
17. A. O. Nier, D. J. Schlutter, D. E. Brownlee, *ibid.* **54**, 173 (1990).
18. J. Matsuda, M. Murota, K. Nagao, *J. Geophys. Res.* **95**, 7111 (1990).
19. C. J. Allègre, P. Sarda, T. Staudacher, *Earth Planet. Sci. Lett.* **117**, 229 (1993).
20. D. L. Anderson, *Science* **261**, 170 (1993).
21. B. K. Esser and K. K. Turekian, *Geochim. Cosmochim. Acta* **52**, 1383 (1988).
22. D. E. Brownlee, *Annu. Rev. Earth Planet. Sci.* **13**, 147 (1985).
23. W. Hunter and D. W. Parkin, *Proc. R. Soc. London, Ser. A* **A255**, 382 (1960).
24. A 200-mesh sieve was used. Both iron and stony IDPs above this size are expected to be melted on entering the atmosphere (*23*).
25. S. Zashu used this technique to avoid reactions between a molybdenum crucible and carbonado diamonds [S. Zashu, thesis, University of Tokyo (1992)].
26. The data may also be interpreted as a change in the activation energies at ~700°C: activation energies are lower at <700°C and higher at >700°C. If this is the case, extrapolation to lower temperatures of the data from fractions ranging from 500° to 700°C would give *D*/*a*^{2} values much higher than those given in the text. This would result in the faster release of solar He and Ne from IDPs, which would strengthen the conclusion of the present study that solar He and Ne would be easily lost from IDPs during the subduction process.
27. T. Futagami, M. Ozima, Y. Nakamura, *Earth Planet. Sci. Lett.* **101**, 63 (1990).
28. W. G. Perkins and D. R. Begal, *J. Chem. Phys.* **54**, 1683 (1971).
29. M. D. Kurz and W. J. Jenkins, *Earth Planet. Sci. Lett.* **53**, 41 (1981).
30. S. R. Hart, *ibid.* **70**, 297 (1984); T. W. Trull and M. D. Kurz, *Geochim. Cosmochim. Acta* **57**, 1313 (1993).
31. H. Martin, *Geology* **14**, 753 (1986); M. Cools, *Geol. Soc. Am. Bull.* **105**, 715 (1993).
32. Y. Tatsumi, *J. Geophys. Res.* **94**, 4697 (1989).

33. I thank K. Yamakoshi for providing the Pacific Ocean sediment; I. Kaneoka and N. Sugiura for valuable discussions; and M. Ozima, J. Matsuda, and D. B. Patterson for valuable comments and suggestions on the manuscript.

30 September 1993; accepted 4 January 1994

Superconducting Mercury-Based Cuprate Films with a Zero-Resistance Transition Temperature of 124 Kelvin

C. C. Tsuei, A. Gupta, G. Trafas, D. Mitzi

The synthesis of high-quality films of the recently discovered mercury-based cuprate films with high transition temperatures has been plagued by problems such as the air sensitivity of the cuprate precursor and the volatility of Hg and HgO. These processing difficulties have been circumvented by a technique of atomic-scale mixing of the HgO and cuprate precursors, use of a protective cap layer, and annealing in an appropriate Hg and O_2 environment. With this procedure, a zero-resistance transition temperature as high as 124 kelvin in *c* axis–oriented epitaxial $HgBa_2CaCu_2O_{6+\delta}$ films has been achieved.

The recent discovery of superconductivity in mercury-based cuprates (*1, 2*) ($HgBa_2Ca_{n-1}Cu_nO_{2n+2+\delta}$) has pushed the superconducting transition temperature (T_c) to values higher than 130 K. More recently, the T_c of Hg-cuprate with $n = 3$ has been reported to increase to 153 K under quasi-hydrostatic pressure (*3*). To put these new materials to effective use in superconducting microelectronic devices—such as in superconducting quantum interference devices (SQUIDs) and microwave applications and in the measurement of their basic intrinsic properties—we must be able to fabricate high-quality thin films. In addition to the experimental complications caused by the severe air sensitivity of the cuprate precursor ($Ba_2Ca_{n-1}Cu_nO_x$), the highly volatile and toxic nature of Hg and HgO makes the synthesis of such films an extremely difficult task.

Recently, Wang *et al.* (*4*) reported the growth of micrometer-thick films of $HgBa_2CaCu_2O_{6+\delta}$ with a magnetically determined T_c of ~120 K. They prepared the films by reacting radio-frequency–sputtered films of $Ba_2CaCu_2O_x$ in a controlled Hg atmosphere. Although a diamagnetic transition was reported, no resistive transition was observed. Clearly, alternative methods for fabricating films with better superconducting characteristics need to be explored.

The difficulties of synthesizing Hg-containing cuprate films mainly stem from the high volatility of Hg and Hg-based compounds. For example, HgO decomposes at ~500°C, whereas the formation of the superconducting phase of Hg-cuprates calls for thermal annealing at 800°C. Similar problems were also encountered in the fabrication of Tl-based cuprate films (*5*), except that Tl_2O_3, the HgO counterpart, is stable up to 800°C. Furthermore, the sticking coefficient of Hg, unlike that of Tl, is vanishingly small unless the substrate temperature during deposition is kept quite low (*6*).

To overcome these experimental difficulties, we developed a technique for the atomic-scale mixing of HgO and the alkaline earth–copper oxide precursor by means of layer-by-layer pulsed laser deposition (PLD). To fabricate films of $HgBa_2CaCu_2O_{6+\delta}$ ($n = 2$) (referred to as Hg-1212), for example, we use the PLD technique to deposit sequential layers of HgO (~5 Å) and $Ba_2CaCu_2O_x$ (~25 Å) from two separate targets. This technique provides a convenient means for controlling the film composition and homogeneity. The films are deposited at room temperature in a vacuum atmosphere (~10^{-6} torr) on (100) $SrTiO_3$ substrates. The film thickness is of the order of 0.5 to 2 μm.

To minimize the detrimental effects of moisture and CO_2 in the air, we deposit

IBM Research Division, Thomas J. Watson Research Center, Yorktown Heights, NY 10598–0218, USA.

a cap layer of 500 to 5000 Å on top of the Hg-cuprate film. The cap layer materials used are HgO, MgO, or $SrTiO_3$. Aside from providing a protective cover, the cap layer also helps retain the Hg in the film during the postannealing step required for formation of the superconducting phase.

We made Rutherford backscattering (RBS) measurements on a $HgBa_2CaCu_2O_x$ film (Fig. 1). The excellent agreement between the theoretical simulation (7) and the experimental data suggests that HgO and the precursor are well mixed and the desired stoichiometric composition has been achieved. The 1800 Å HgO protective cap layer manifests itself as a peak at 2.1 MeV.

The laser-deposited films are mostly amorphous and have to be annealed at high temperatures to form the superconducting phase. The films are annealed in a carefully controlled Hg atmosphere at a precise temperature and O_2 partial pressure that are consistent with the thermodynamic requirements for stabilizing the high T_c phase. We accomplished this by enclosing the Hg-cuprate film in an evacuated quartz tube (length, 7 cm; inner diameter, 0.7 cm) with appropriate amounts of bulk unreacted, stoichiometric Hg-cuprate and pellets of the precursor ($Ba_2CaCu_2O_x$). The amounts of the bulk Hg-cuprate (*X*) and precursor (*P*) materials by weight needed to achieve the appropriate Hg and O_2 overpressure at the annealing temperature depend sensitively on the size of the quartz tube and other factors such as the annealing temperature and film composition. Our best results were obtained with $X/P = 2$. A typical annealing schedule consists of slow heating at 150°C/hour to 750° to 810°C, which is sustained for 1 hour, followed by a furnace cooling to room temperature (~6 hours).

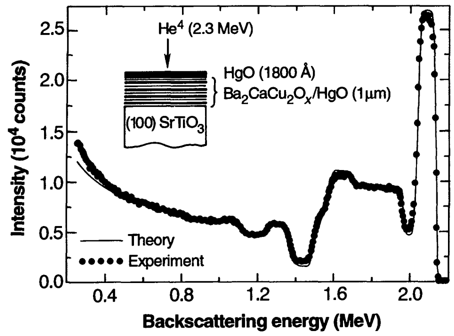

Fig. 1. The RBS intensity as a function of the backscattering energy for a film of Hg-1212 (1 µm thick) capped with a 1800 Å HgO layer.

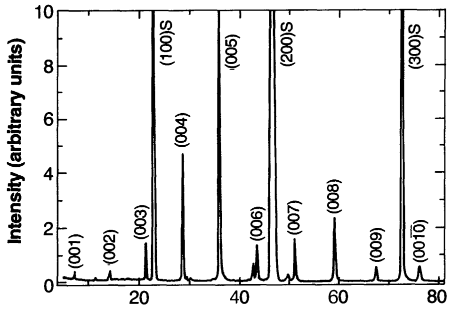

Fig. 2. The XRD pattern for a Hg-1212 film (1.5 µm thick with 500 Å MgO cap layer) annealed at 800°C for 1 hour with $X/P = 2$. The substrate peaks in the pattern are denoted by S.

The x-ray diffraction (XRD) pattern shown in Fig. 2 indicates that nearly phase-pure Hg-1212 films can be obtained after the annealing step (800°C for 1 hour). The diffraction peaks for the small amounts of impurity phases (<2%) correspond primarily to the single-layer Hg-1201 phase. The films are epitaxially aligned with the *c* axis, normal to the substrate plane. The *c* axis lattice parameter varies to some extent with the annealing treatment and has been observed to be in the range of 12.48 to 12.60 Å. This is somewhat smaller than the value observed in the bulk (12.71 Å).

The electrical resistance as a function of temperature, *R*(*T*), for a *c* axis–oriented $HgBa_2CaCu_2O_{6+\delta}$ epitaxial film (annealed at 775°C for 1 hour) is characterized by a sharp transition with a zero-resistance T_c of 124 K (Fig. 3). The ac magnetic susceptibility $\chi(T)$ (Fig. 3, inset) indicates an equally sharp transition starting at 124 K. Most of the Hg-1212 films we have prepared so far show zero-resistance transition temperatures between 115 and 120 K. As observed in other high T_c cuprates such as $YBa_2Cu_3O_7$, the normal state resistance depends linearly on temperature with some rounding near T_c, possibly because of thermodynamic fluctuations. The resistance ratio $R(300\ K)/R(T \geq T_c) \sim 3$ is comparable with that of high-quality single crystals of $YBa_2Cu_3O_7$. The room-temperature resistivity of the film has been estimated to be ~400 microhm·cm, which is substantially lower than that measured in bulk polycrystalline samples (8) and is similar to what is observed in other high T_c cuprates. This Hg-based cuprate film was annealed at 775°C with $X/P = 2$ and without the need for any postoxygenation.

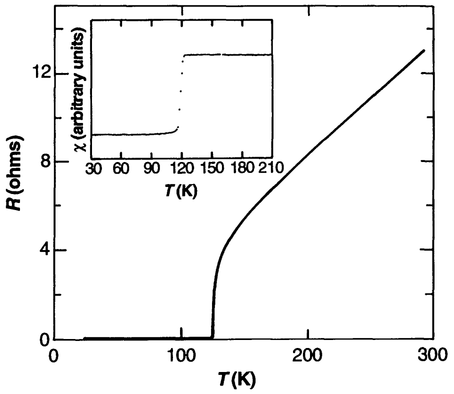

Fig. 3. Electrical resistance as a function of temperature for the Hg-1212 film whose as-deposited RBS spectra is shown in Fig. 1. (**Inset**) The inductive component of the ac susceptibility for this film. The film was annealed at 775°C for 1 hour with $X/P = 2$.

Preliminary zero-field-cooled and field-cooled magnetization (M) measurements on the Hg-1212 films with $T_c \lesssim 120$ K indicate that the superconducting shielding effect is nearly 100% and the Meissner effect is of the order of 3 to 5%, suggesting relatively strong flux pinning. To estimate the magnitude of critical current density J_c, we measured the *M*-*H* loop for a Hg-1212 film with $T_c = 117$ K (Fig. 4). Using the remnant magnetization, at 10 K and 77 K, and the Bean formula, one obtains lower bound estimates for J_c of $\sim 3 \times 10^5$ A/cm^2 at $T = 10$ K and $\sim 5 \times 10^4$A/cm^2 at $T = 77$ K. In calculating these numbers, we used the total area covered by the film (5 mm by 2 mm) rather than the grain size. Estimates using grain size would result in J_c values one to two orders of magnitude higher, which would then be similar to those observed for other high T_c cuprates.

Many device applications are limited by the degree of roughness on the film surface. There are no substantial data on the surface morphology of the Hg-cuprate films made in this work. However, some of our films appear mirror-like, similar to our high-quality $YBa_2Cu_3O_7$ films, suggesting smooth surfaces. A preliminary surface roughness measurement on a Hg-1212 film (the one used for Fig. 2) by

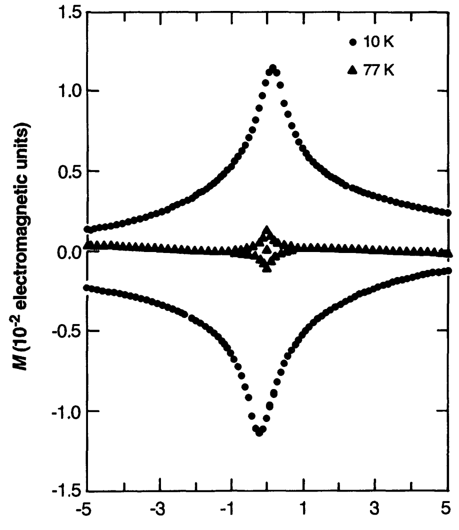

Fig. 4. The *M*-*H* loop at 10 K (●) and 77 K (▲) for a Hg-1212 film with a zero-resistance T_c of 117 K. The magnetic field is perpendicular to the film plane (that is, *H* is parallel to the *c* axis).

an alpha-step surface profilameter indicates that variations in surface roughness typically range from 100 to 500 Å over a scan length of 1 mm. Variations as large as a few thousand angstroms can be spotted occasionally. These preliminary results are very encouraging for potential superconducting device applications. It is hoped that in the future, thinner and optimized films will have even better surface morphology.

The synthesis of high-quality Hg-cuprate films has posed one of the toughest challenges so far in the area of high T_c films because of the highly volatile nature of Hg-based compounds. Various standard thin-film techniques for volatile materials failed to achieve high-quality Hg-cuprate films. Only after the adoption of multitarget atomic-scale mixing, cap layers, and controlled annealing techniques were such films achieved reproducibly. The atomic-scale mixing and the protective cap layer ensure stoichiometric composition before annealing. The as-deposited films prepared by Wang *et al.* (4) contained no Hg at all and required diffusion of Hg into the film after deposition. This procedure is likely to be more prone to film inhomogeneity, especially degradation at the grain boundaries, which may account for the lack of electrical connectivity in their films. In addition, given the high volatility of Hg compounds, the use of a single stoichiometric target (which was also tried) leads to insulating films, almost certainly because of preferential deposition.

Our approach provides for a precise control of the Hg content in the film, which is key to success. In a more general sense, the technique presented in this work is expected to find more general applications in the synthesis of thin films containing volatile materials other than mercury. In view of their excellent electrical and magnetic characteristic, these films are expected to be useful in applications of Josephson junctions such as grain boundary SQUIDs and other devices.

REFERENCES AND NOTES

1. S. N. Putilin, E. V. Antipov, O. Chmaissem, M. Marezio, *Nature* **362**, 226 (1993).
2. A. Schilling, M. Cantoni, J. D. Guo, H. R. Ott, *ibid.* **363**, 56 (1993).
3. C. W. Chu *et al.*, *ibid.* **365**, 323 (1993).
4. Y. Q. Wang *et al.*, *Appl. Phys. Lett.* **63**, 3084 (1993).
5. W. Y. Lee *et al.*, *ibid.* **60**, 772 (1992).
6. C. A. Neugebauer, in *Handbook of Thin Film Technology*, L. I. Maissel and R. Glang, Eds. (McGraw Hill, New York, 1970), pp. 8–22.
7. P. A. Saunders and J. F. Ziegler, *Nucl. Instrum. Methods Phys. Res.* **218**, 67 (1983).
8. R. L. Meng *et al.*, *Phys. C* **216**, 21 (1993).

9. We thank G. Coleman, C. Feild, P. Duncombe, and E. Kummer for their technical assistance and A. Guloy, C. C. Chi, B. Mercey, M. Ketchen, and B. A. Scott for helpful discussions. Supported in part by the Defense Advanced Research Projects Agency under contract N00014-89-0112.

9 December 1993; accepted 6 January 1994

Atomic Force Microscopy of the Electrochemical Nucleation and Growth of Molecular Crystals

Andrew C. Hillier and Michael D. Ward*

In situ atomic force microscopy reveals the morphology, surface topography, and growth and dissolution characteristics of microscopic single crystals of the low-dimensional organic conductor (tetrathiafulvalene)$Br_{0.76}$, which are grown by electrocrystallization on a highly oriented pyrolytic graphite electrode in an atomic force microscope liquid cell. The growth modes and the distribution and orientation of topographic features on specific crystal faces, whose identity was determined by "atomic force microscope goniometry," can be correlated with the strength and direction of anisotropic solid-state intermolecular bonding. Growth on the (011) face of (tetrathiafulvalene)$Br_{0.76}$ crystals involves the formation of oriented self-similar triangular islands ranging in size from 200 to 5000 angstroms along a side. These nuclei eventually transform into rectangular rafts at larger length scales, where bulk intermolecular bonding interactions and surface energies dominate over nuclei-substrate interactions.

Molecular crystals containing organic components exhibit a variety of electronic properties, including electrical conductivity, superconductivity, nonlinear optical behavior, and ferromagnetism (*1*), and also comprise the majority of pharmaceutical reagents (*2*). Much of the interest in these materials stems from the ability to use molecular-level "crystal engineering" strategies (*3*) to control solid-state intermolecular interactions in order to rationally manipulate crystal packing and, consequently, influence bulk physical and electronic properties. Although these strategies have been used in the design and synthesis of many organic crystals, the self-assembly, nucleation, and crystallization processes that are responsible for their formation are not well understood, particularly at the molecular level and nanometer length scales. This understanding is crucial if important crystal characteristics such as polymorphism, morphology, inclusion formation, and defect density are to be controlled.

Recent developments in atomic force microscopy (AFM) (*4*), however, now provide for in situ visualization of the early stages of growth of organic crystals in liquids (*5–7*). This capability allows dynamic observation of nucleation events and the determination, at small length scales, of the distribution of topographic features (that is, terraces, ledges, and kinks) that play an important role in crystal growth (*8*). We made in situ AFM observations of the electrochemical nucleation and growth of the crystalline quasi–one-dimensional organic conductor (TTF)$Br_{0.76}$ (TTF, tetrathiafulvalene) (*9*), wherein the rate of crystal growth was regulated by the electrochemical potential applied during the electrocrystallization process (*10*). Electrocrystallization is a convenient method for AFM visualization of crystal growth modes because the supersaturation at the crystal surface can be controlled by the electrochemical potential, analogous to the effect of changing solute concentration during the growth of nonconducting crystals. We chose (TTF)$Br_{0.76}$ because it is representative of low-dimensional organic conductors and previous studies (*11*) indicated that growth occurred readily on existing nuclei during electrocrystallization.

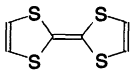

TTF

Electrochemical nucleation and growth of well-defined needle crystals of the conductive, nonstoichiometric salt (TTF)$Br_{0.76}$ on a freshly cleaved, highly oriented pyrolytic graphite (HOPG) electrode was accomplished readily in an AFM liquid cell (*12*). Crystallization was induced by the brief application (1 to 5 s) of an anodic potential step in the range $0.40 \leq E_{\text{applied}} \leq 0.70$ V [versus a saturated calomel electrode (SCE)] (*13*). Under these conditions, AFM revealed nucleation of (TTF)$Br_{0.76}$ crystals on the HOPG electrode, with nucleation densities approaching 10^3 mm^{-2}. These needle crystals exhibited widths ranging from 0.2 to 4 μm, lengths of 10 to 15 μm, and heights of 0.1 to 0.75 μm. The needle axis of the

---

Department of Chemical Engineering and Materials Science, University of Minnesota, Amundson Hall, 421 Washington Avenue, S.E., Minneapolis, MN 55455, USA.

*To whom correspondence should be addressed.